

Topology optimization of material-nonlinear continuum structures by the element connectivity parameterization

Gil Ho Yoon and Yoon Young Kim^{*,†}

Multiscale Design Center and Integrated Design & Analysis of Structures Laboratory, School of Mechanical and Aerospace Engineering, Seoul National University, Kwanak-Gu San 56-1, Seoul 151-742, Korea

SUMMARY

The application of the element density-based topology optimization method to nonlinear continuum structures is limited to relatively simple problems such as bilinear elastoplastic material problems. Furthermore, it is very difficult to use analytic sensitivity when a commercial nonlinear finite element code is used. As an alternative to the element density formulation, the element connectivity parameterization (ECP) formulation is developed for the topology optimization of isotropic-hardening elastoplastic or hyperelastic continua by using commercial software. ECP varies the stiffness of zero-length linear elastic links that connect design domain-discretizing finite elements. Unloading was not considered. But the advantages of ECP in material-nonlinear problems were demonstrated: considerably simple analytic sensitivity calculation using a commercial code and simple link stiffness penalization regardless of nonlinear material behaviour. Copyright © 2006 John Wiley & Sons, Ltd.

Received 7 October 2005; Revised 15 June 2006; Accepted 19 June 2006

KEY WORDS: topology optimization; material-nonlinearity; element connectivity parameterization

1. INTRODUCTION

The topology optimization method has been successful in many applications [1, 2], but the topology optimization of some structural problems involving nonlinearity still needs further development. Though the topology design optimization of frame structures involving plasticity was studied [3–5], the topology design optimization of elastoplastic continuum bodies still remains difficult [6–11]. In this work, the topology optimization of material-nonlinear continuum bodies will be solved by the element connectivity parameterization (ECP) method [12–14], a recently developed method. Although isotropic-hardening elastoplastic or hyperelastic material behaviour without unloading

^{*}Correspondence to: Yoon Young Kim, Multiscale Design Center and Integrated Design & Analysis of Structures Laboratory, School of Mechanical and Aerospace Engineering, Seoul National University, Kwanak-Gu San 56-1, Seoul 151-742, Korea.

[†]E-mail: yykim@snu.ac.kr

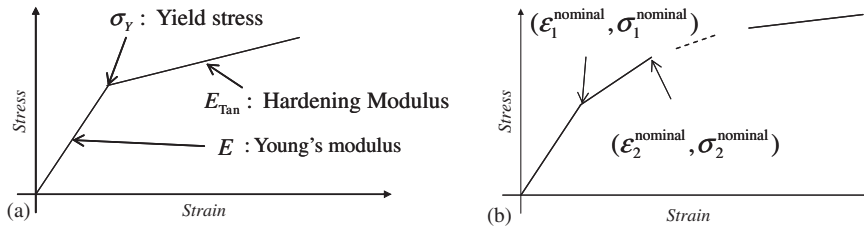


Figure 1. Nonlinear material models: (a) bilinear elastoplastic case; and (b) multilinear elastoplastic case.

will be considered in this investigation, the advantage of the ECP method in dealing with material-nonlinear problems can be clearly demonstrated. The ECP formulation for material-nonlinear problems and the analytic sensitivity will be presented in this investigation.

When the conventional element density approach in material-nonlinear problems is used, the density-dependent material penalization and the analytic sensitivity analysis become considerably complicated. In the literatures (see, References [8–10, 15]), the analytic sensitivity was given only for simple elastoplastic models such as the bilinear elastoplastic material shown in Figure 1(a). When the density method is used for the bilinear elastoplastic material model, three material properties, Young's modulus (E), the hardening modulus (E_{Tan}), and the yield stress (σ_Y), may be interpolated as the functions of the element density variable (ρ_e). For instance, the following interpolations may be used [9–11]:

$$E^e(\rho_e) = E\rho_e^{\beta_1}, \quad E_{\text{Tan}}^e(\rho_e) = E_{\text{Tan}}\rho_e^{\beta_2}, \quad \sigma_Y^e(\rho_e) = \sigma_Y\rho_e^{\beta_3} \quad (1)$$

The penalization model in Equation (1) is similar to that used for linear elasticity but a right combination of penalty exponents ($\beta_1, \beta_2, \beta_3$) must be used for stable numerical convergence [7, 9]. So far, no rule to determine the relative ratios of these exponents has been developed. The same penalty exponent for the general nonlinear material was employed in Reference [7], but no analytic sensitivity was derived.

It is known that even the optimized topological layouts of linear continua are affected by the choice of the penalty exponents because of many local optima [1, 2, 13]. In case of material-nonlinear problems, the situation can become worse [7, 9]. The difficulty of deriving and calculating analytic sensitivity in problems involving material-nonlinearity cannot be overlooked when the standard element density method is employed [8, 15, 16]. Furthermore, the density method requires an access to a finite element source code for analytic sensitivity; commercial finite element packages may not be used in general. (The direct finite-differencing sensitivity analysis is out of consideration as it requires a tremendous amount of computation time.) More discussions on the design optimization of nonlinear structures may be found in References [4, 7, 8, 15–18].

Our key idea for the efficient topology optimization of material-nonlinear continua is to use a new topology optimization formulation suitable for material-nonlinear problems instead of the standard element density-based formulation. Specifically, we adopt the element connectivity parameterization (ECP) method to formulate the topology optimization of material-nonlinear problems [12]. ECP has been developed for the topology optimization of geometrically nonlinear structures having linear elastic materials in order to resolve the numerical instability caused by low-density elements [12]. It has been recently shown that the ECP formulation is also successful in multiphysics problems involving heat transfer [13] and dynamic problems [19]. In the ECP

formulation, the element material properties remain unchanged during the whole optimization process even if structural topologies vary. Structural layouts are represented by the degrees of the inter-element connectivity that are modelled by one-dimensional zero-length links connecting element nodes. This means that the stiffness of the element-connecting links is varied unlike in the element density method varying the stiffness of the discretizing continuum elements; very flexible links represent virtually disconnected inter-element states whereas very stiff links represent rigidly connected inter-element states. To obtain a solid-void optimal solution, the link stiffness is treated as a penalized function of a design variable that is assigned to every link or a group of links [12, 13].

In employing the ECP approach for material-nonlinear problems, we propose the use of one-dimensional *linear elastic* links, not nonlinear links. Though nonlinear materials are considered, there is no need to use nonlinear links because the links are used to represent the element connectivity only. Indeed, this characteristic is crucial in simplifying the whole topology optimization process. Even in case of the multilinear elastoplastic model in Figure 1(b), only the stiffness of the linear elastic link is varied as the function of the design variable regardless of the adopted nonlinear system. Furthermore, exactly the same formulation applies to any material-nonlinear problem. In the ECP formulation of material-nonlinear problems, the system stiffness matrix consists of two parts: the link stiffness matrix and the discretizing finite element stiffness matrix [13]. It should be emphasized that only the link stiffness matrix depends explicitly on the design variable. Because the sensitivity analysis of implicitly depending terms can be converted to a problem to solve structural response by the adjoint variable approach, any commercial finite element package providing nonlinear analysis can be employed. The explicit sensitivity analysis using commercial software was developed in the present investigation. In our implementation, ANSYS [20] was used for all numerical analyses including the sensitivity analysis.

In the present development, two types of material-nonlinear problems including elastoplastic problems were solved, but unloading was not considered. First, isotropic-hardening elastoplastic cases with small displacement assumption were considered. After verifying the validity of the present formulation in bilinear elastoplastic problems, multilinear elastoplastic problems were solved by the proposed formulation. To authors' knowledge, the multilinear elastoplastic case in continuum structures by using the analytical sensitivity is solved here for the first time. The second set of problems involves the Mooney–Rivlin hyper-elastic materials with the consideration of kinematic nonlinearity. To demonstrate the modelling advantage of the ECP formulation, a design problem involving simple contact was also considered [17, 21–25].

2. ELEMENT CONNECTIVITY PARAMETERIZATION FOR MATERIAL-NONLINEAR PROBLEMS

2.1. Summary of field equations for nonlinear materials

There are several mathematical models to describe elastoplastic material behaviour [26, 27]. Among them, the Prandtl–Reuss incremental formulation of two-dimensional elastoplastic materials will be employed. In this work, unloading will not be considered. The detailed finite element implementation of the elastoplastic analysis can be found in Reference [27]. Although the method to be proposed works also for large displacement, only small displacement will be considered as in References [12, 28, 29].

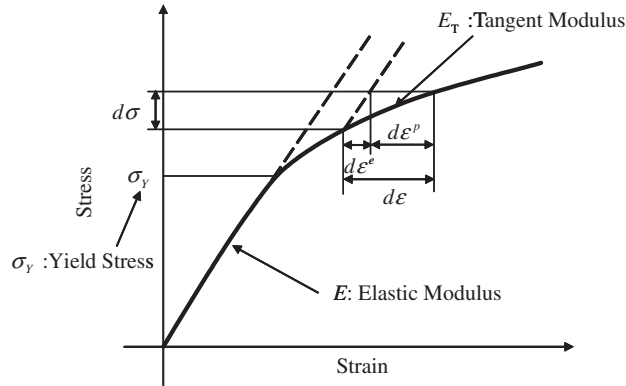


Figure 2. The elastoplastic material behaviour for the uniaxial case.

The linear elastic constitutive relation for a two-dimensional plane stress condition can be expressed as

$$\boldsymbol{\sigma} = \mathbf{D}\boldsymbol{\varepsilon}; \quad \mathbf{D} = \frac{E}{1-\nu^2} \begin{bmatrix} 1 & \nu & 0 \\ \nu & 1 & 0 \\ 0 & 0 & \frac{1-\nu}{2} \end{bmatrix} \quad (2)$$

where E and ν are Young's modulus and Poisson's ratio, respectively. The stress $\boldsymbol{\sigma}$ and the strain $\boldsymbol{\varepsilon}$ consist of three components.

For elastoplastic materials, the stress–strain relation in the following incremental form is used:

$$d\boldsymbol{\sigma} = \mathbf{D}_{EP} d\boldsymbol{\varepsilon} \quad (3)$$

To write the matrix \mathbf{D}_{EP} explicitly, the total incremental strain is decomposed into the incremental elastic strain ($d\boldsymbol{\varepsilon}^e$) and the incremental plastic strain ($d\boldsymbol{\varepsilon}^p$). If we assume that the stress–strain relation for the uniaxial tension experiment of an elastoplastic material is given by a curve H in Figure 2 and the Prandtl–Reuss formulation (see, e.g. References [26, 27]), the plasticity materials, \mathbf{D}_{EP} in (3) will become

$$\mathbf{D}_{EP} = \mathbf{D} - \frac{\mathbf{d}_D \mathbf{d}_D^T}{\dot{H} + \mathbf{d}_D^T \mathbf{a}} \quad (4)$$

$$\mathbf{d}_D^T = \mathbf{a}^T \mathbf{D} \quad \text{and} \quad \mathbf{a}^T = \frac{\partial G}{\partial \boldsymbol{\sigma}} \quad (5)$$

$$G(\boldsymbol{\sigma}, \kappa) = f(\boldsymbol{\sigma}) - \sigma_Y(\kappa) = 0 \quad (6)$$

where σ_Y is the yield stress shown in Figure 2 and κ is the hardening parameter [27]. The yield function is denoted by $f(\boldsymbol{\sigma})$.

2.1.1. Finite element expression. As the equilibrium equation, the following principal virtual work will be used:

$$0 = \lambda_{LF} \int_{\Gamma} \delta \mathbf{u}^T \hat{\mathbf{t}} d\Gamma - \int_{\Omega} \delta \boldsymbol{\varepsilon}^T \boldsymbol{\sigma} d\Omega \quad (7)$$

where $\hat{\mathbf{t}}$ and λ_{LF} are the traction vector and the load factor on the traction boundary Γ , respectively. The analysis domain is denoted Ω . The test displacement and the corresponding test strain are denoted by $\delta \mathbf{u}$ and $\delta \boldsymbol{\varepsilon}$, respectively. In this paper, the body force is neglected.

Following the procedure given in Reference [27], the nodal displacement (\mathbf{U}) for finite element analysis can be written as

$$\mathbf{U}^{(k+1)} = \mathbf{U}^{(k)} + d\mathbf{U} \quad (8)$$

where the right superscript k is the Newton–Raphson iteration number and $d\mathbf{U}$ is the incremental displacement computed from

$$\mathbf{K}_{\text{Tan}} d\mathbf{U} = \mathfrak{R}(\mathbf{U}^{(k)}) \quad (9)$$

$$\mathfrak{R}(\mathbf{U}^{(k)}) = \lambda_{LF} \int_{\Gamma} \mathbf{H}^T \hat{\mathbf{t}} d\Gamma - \int_{\Omega} \mathbf{B}^T \boldsymbol{\sigma}(\mathbf{U}^{(k)}) d\Omega \quad (10)$$

where \mathbf{K}_{Tan} is the tangent stiffness matrix for the discretized system. It is defined in the discretized solution space as

$$\mathbf{K}_{\text{Tan}} = \sum_{e=1}^{\text{NE}} \int_{\Omega_e} \mathbf{B}^T \mathbf{D}_{\text{EP}} \mathbf{B} d\Omega_e \quad (11)$$

where NE is the total number of finite elements and Ω_e is the e th element domain. In the above equations, \mathbf{B} and \mathbf{H} are the strain–displacement matrix and the displacement transformation matrix, respectively.

2.2. Density-based optimization formulation for the elastoplastic material case

Before developing the ECP based topology optimization method for nonlinear structures, the conventional framework of the density-based optimization is presented in this section.

In the element density-based formulation, a density design variable ρ_e ($e = 1, \dots, \text{NE}$) varying between 0 and 1 is assigned to every finite element. In References [7, 9, 10], the following optimization setup or an equivalent setup was used. In this case, the optimization problem may be stated as

$$\text{minimize} \quad \Phi(\boldsymbol{\rho}) = - \int_{\Omega} \int_{\hat{\varepsilon}} \boldsymbol{\sigma}^T d\boldsymbol{\varepsilon} d\Omega \quad (12a)$$

$$\text{subject to} \quad \mathbf{Q}(\boldsymbol{\rho}) = \sum_{e=1}^{\text{NE}} \rho_e v_e - M_0 \leq 0 \quad (12b)$$

$$\mathfrak{R}(\mathbf{U}, \boldsymbol{\rho}) = 0 \quad (\text{Equilibrium}) \quad (12c)$$

$$\boldsymbol{\rho} = \{\rho_1, \rho_2, \dots, \rho_{\text{NE}}\}^T$$

where M_0 and v_e are the mass limit and the e th element volume, respectively. In (12a), the symbol $\hat{\epsilon}$ denotes the strain corresponding to the prescribed displacement boundary condition \hat{u} . In (12c), \mathbf{U} stands for the converged displacement and the residual \mathfrak{R} becomes dependent on the design variables ρ . In Equation (12a), $\int_{\Omega} \int_{\hat{\epsilon}} \boldsymbol{\sigma}^T d\boldsymbol{\epsilon} d\Omega$ denotes ductility so that (12a) implies the maximization of the total strain.

To facilitate the sensitivity analysis, two assumption are employed [8, 10]; unloading will not take place and the loading is controlled by the prescribed monotonic displacements. Using the variational adjoint formulation, the sensitivity of the objective function with respect to the design variable ρ_e becomes

$$\begin{aligned} \frac{\partial \Phi}{\partial \rho_e} &= -\frac{\partial}{\partial \rho_e} \int_{\Omega_e} \int_{\hat{\epsilon}} \boldsymbol{\sigma}^T d\boldsymbol{\epsilon} d\Omega = -\frac{\partial}{\partial \rho_e} \int_{\Omega_e} \int_{\hat{\epsilon}} \int_{\boldsymbol{\sigma}} d\boldsymbol{\sigma}^T d\boldsymbol{\epsilon} d\Omega \\ &= -\int_{\Omega_e} \int_{\hat{\epsilon}} \int_{\boldsymbol{\sigma}} \frac{\partial(d\boldsymbol{\sigma}^T)}{\partial \rho_e} d\boldsymbol{\epsilon} + d\boldsymbol{\sigma}^T \frac{\partial(d\boldsymbol{\epsilon})}{\partial \rho_e} d\Omega \end{aligned} \quad (13a)$$

$$= -\int_{\Omega_e} \int_{\hat{\epsilon}} \int_{\boldsymbol{\sigma}} d\boldsymbol{\epsilon}^T \frac{\partial(\mathbf{D}_{EP})}{\partial \rho_e} d\boldsymbol{\epsilon} + 2 \left(\frac{\partial(d\boldsymbol{\epsilon})}{\partial \rho_e} \right)^T \mathbf{D}_{EP} d\boldsymbol{\epsilon} d\Omega \quad (13b)$$

$$= -\int_{\Omega_e} \int_{\hat{\epsilon}} \int_{\boldsymbol{\epsilon}} d\boldsymbol{\epsilon}^T \frac{\partial \mathbf{D}_{EP}}{\partial \rho_e} d\boldsymbol{\epsilon} d\Omega \quad (13c)$$

To obtain (13b), we used the following relation:

$$\frac{\partial(d\boldsymbol{\sigma})}{\partial \rho_e} = \frac{\partial(\mathbf{D}_{EP})}{\partial \rho_e} d\boldsymbol{\epsilon} + \mathbf{D}_{EP} \frac{\partial(d\boldsymbol{\epsilon})}{\partial \rho_e} \quad (14)$$

To derive Equation (13c), the condition of monotonic displacement loading, $d\mathbf{u}^T \hat{\mathbf{t}} = \hat{\mathbf{t}}^T d\mathbf{u} = \text{constant}$, is used for the differentiation of the incremental equilibrium equation (7) [10]:

$$\int_{\Gamma} \int_{\hat{\lambda}_{LF}} \int_{\hat{\mathbf{u}}} \frac{\partial(d\lambda_{LF} \hat{\mathbf{t}}^T)}{\partial \rho_e} d\mathbf{u} d\Gamma - \int_{\Omega} \int_{\hat{\epsilon}} \int_{\boldsymbol{\epsilon}} d\boldsymbol{\epsilon}^T \left(\frac{\partial \mathbf{D}_{EP}}{\partial \rho_e} d\boldsymbol{\epsilon} + \mathbf{D}_{EP} \frac{\partial d\boldsymbol{\epsilon}}{\partial \rho_e} \right) d\Omega = 0 \quad (15a)$$

$$\frac{\partial d\lambda_{LF}}{\partial \rho_e} = \int_{\Omega} d\boldsymbol{\epsilon}^T \frac{\partial \mathbf{D}_{EP}}{\partial \rho_e} d\boldsymbol{\epsilon} d\Omega / d\mathbf{u}^T \hat{\mathbf{t}} \quad (15b)$$

where $\hat{\lambda}_{LF}$ is the load factor due to the input displacement loading. Because the load $\hat{\mathbf{t}}$ is not dependent on the design variables, Equation (15a) can be simplified to Equation (15b).

Equation (13c) indicates that the analytic sensitivity of $\partial \Phi / \partial \rho_e$ requires the explicit evaluation of $\partial \mathbf{D}_{EP} / \partial \rho_e$. In References [4, 5, 8–11], the analytic sensitivity was used only in case of ‘bilinear’ elastoplastic materials. Even in the bilinear case, the sensitivity analysis would require material-dependent analysis as may be seen in the following equation:

$$\begin{aligned} \frac{\partial \mathbf{D}_{EP}}{\partial \rho_e} &= \frac{\partial \mathbf{D}_{EP}}{\partial E^e} \frac{\partial E^e}{\partial \rho_e} + \frac{\partial \mathbf{D}_{EP}}{\partial E_{Tan}^e} \frac{\partial E_{Tan}^e}{\partial \rho_e} + \frac{\partial \mathbf{D}_{EP}}{\partial \sigma_Y^e} \frac{\partial \sigma_Y^e}{\partial \rho_e} \\ &= \frac{\partial \mathbf{D}_{EP}}{\partial E^e} (\beta_1 E \rho_e^{\beta_1-1}) + \frac{\partial \mathbf{D}_{EP}}{\partial E_{Tan}^e} (\beta_2 E_{Tan} \rho_e^{\beta_2-1}) + \frac{\partial \mathbf{D}_{EP}}{\partial \sigma_Y^e} (\beta_3 \sigma_Y \rho_e^{\beta_3-1}) \end{aligned} \quad (16)$$

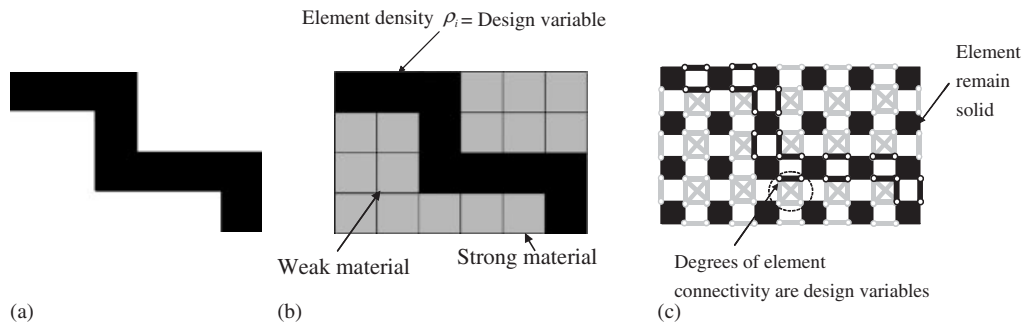


Figure 3. Layout modelling by the density method and the ECP method: (a) an example for the layout configuration; (b) the modelling method by SIMP approach; and (c) the modelling method by the ECP method.

where the material interpolations were based on Equation (1) and the procedure to calculate $\partial \mathbf{D}_{EP} / \partial \rho_e$, $\partial \mathbf{D}_{EP} / \partial E_{\text{Tan}}^e$, $\partial \mathbf{D}_{EP} / \partial \sigma_Y^e$ may be found in References [8, 10, 15]. Note that to simplify the numerical analysis, the term $\partial \mathbf{D}_{EP} / \partial \sigma_Y^e$ was often ignored [8, 10].

When the density based method is used, interpolating each of E^e , E_{tan}^e and σ_Y^e by different parameters β_i may be needed for stable solution convergence. However, choosing an appropriate combination of these parameters may not be trivial [7, 9, 10]. In addition, $\partial \mathbf{D}_{EP} / \partial \rho_e$ should be also calculated. Because the density method varies the material properties of the discretizing elements, there complexities may not be avoided.

If general nonlinear material models other than the bi-linear elastoplastic material should be considered, the sensitivity analysis becomes considerably more difficult compared with the linear material. For instance, when the above-mentioned density-based interpolation scheme is employed for the case of the multilinear material model in Figure 1(b), the sensitivity expression in (16) will involve. Therefore, it appears difficult to use the element density method for the topology optimization of general nonlinear materials.

2.3. Overview of the element connectivity parameterization (ECP)

Before presenting the topology optimization formulation of continuum structures exhibiting material-nonlinearity, the underlying concept of the element connectivity parameterization will be briefly presented.

For a given design domain, the element density based method represents all possible topological layouts by varying element densities. In the ECP formulation, however, a different modelling technique is used; the finite elements discretizing a design domain are assumed to be connected by a set of one-dimensional zero-length elastic links and the link stiffness is varied to represent all possible topological layouts. For example, a two-dimensional structural layout in Figure 3(a) is represented by the model shown in Figure 3(b) in the element density-based method. However, the layout is represented by the model in Figure 3(c) when the ECP formulation is employed.

As illustrated in Figure 3(b), the conventional element density based topology optimization assigns the original strong materials to structural parts, and weak materials to void regions. In

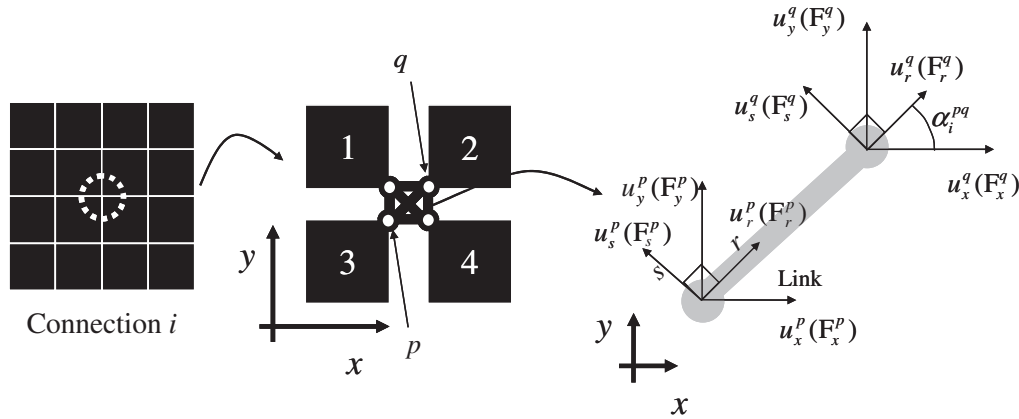


Figure 4. Modelling technique by the ECP method.

the ECP method, however, the whole design domain is discretized by plane finite elements having the original material property and the topological layout of Figure 3(a) is represented by the finite elements weaved by zero-length links having varying stiffness. Links in Figure 3(c) have no length for the actual numerical calculation, but the links in Figure 3(c) have finite lengths for easier visualization of the ECP modelling. The essential feature of the ECP method is that the material properties of the discretizing finite elements are not varied or interpolated; they remain to have the original material property throughout the whole topology optimization process.

To describe the ECP modelling technique numerically, consider the elements around Connection i as shown in Figure 4. Here, the terminology 'Connection' is used to denote the global node where adjacent four finite elements are connected by elastic links. Any pair of the four elements around Connection i can be connected by a one-dimensional elastic link, in which the degree of the inter-element connectivity is controlled by the value of the link stiffness.

In two-dimensional situations, every node defining links has two degrees of freedom. Therefore, the one-dimensional zero-length link connecting nodes p and q can be assumed to have the following link stiffness matrix $k_{i,(p,q)}^{\text{link}}$:

$$\begin{Bmatrix} F_x^p \\ F_y^p \\ F_x^q \\ F_y^q \end{Bmatrix} = k_{i,(p,q)}^{\text{link}} \begin{Bmatrix} u_x^p \\ u_y^p \\ u_x^q \\ u_y^q \end{Bmatrix}; \quad k_{i,(p,q)}^{\text{link}} = l_i^{pq} k_{\text{nominal}}^{\text{link}} = l_i^{pq} \begin{bmatrix} 1 & 0 & -1 & 0 \\ 0 & 1 & 0 & -1 \\ -1 & 0 & 1 & 0 \\ 0 & -1 & 0 & 1 \end{bmatrix} \quad (17)$$

To facilitate the sensitivity analysis for the material-nonlinear problem, as shall be seen later, it may be convenient to treat the zero-length link as the limit of a one-dimensional finite-length elastic link. Referring to Figure 4, consider a link of length L_i^{pq} , the link connecting nodes p and q at Connection i . Based on the local co-ordinates r and s , the stiffness matrix of the link element

$\bar{k}_{i,(p,q)}^{\text{link}}$ may be given by

$$\begin{Bmatrix} F_r^p \\ F_s^p \\ F_r^q \\ F_s^q \end{Bmatrix} = \bar{k}_{i,(p,q)}^{\text{link}} \begin{Bmatrix} u_r^p \\ u_s^p \\ u_r^q \\ u_s^q \end{Bmatrix}; \quad \bar{k}_{i,(p,q)}^{\text{link}} = \lim_{\substack{L_i^{pq} \rightarrow 0 \\ (\Omega_i^{pq} \rightarrow 0)}} \int_{\Omega_i^{pq}} \mathbf{B}^T \mathbf{D}_i^{pq} \mathbf{B} d\Omega \quad (18)$$

where Ω_i^{pq} is the region occupied by the link and $d\Omega = A_i^{pq} dr$ (A_i^{pq} : link cross-sectional area). In (18), $F_{(\Delta)}^{(\Psi)}$ and $u_{(\Delta)}^{(\Psi)}$ denote the nodal forces and the nodal displacement component of node Ψ in the direction of Δ . The conversion from $\bar{k}_{i,(p,q)}^{\text{link}}$ to $k_{i,(p,q)}^{\text{link}}$ is simply given by

$$k_{i,(p,q)}^{\text{link}} = \begin{bmatrix} T_{\alpha_i^{pq}} & 0 \\ 0 & T_{\alpha_i^{pq}} \end{bmatrix}^T \bar{k}_{i,(p,q)}^{\text{link}} \begin{bmatrix} T_{\alpha_i^{pq}} & 0 \\ 0 & T_{\alpha_i^{pq}} \end{bmatrix} \quad \text{with } T_{\alpha_i^{pq}} = \begin{bmatrix} \cos \alpha_i^{pq} & -\sin \alpha_i^{pq} \\ \sin \alpha_i^{pq} & \cos \alpha_i^{pq} \end{bmatrix} \quad (19)$$

where α_i^{pq} is the angle between the r -axis and the x -axis. Now let us assume the displacements $u_r(r, s)$ and $u_s(r, s)$ as

$$u_r(r) = h_r^p(r)u_r^p + h_r^q(r)u_r^q, \quad u_s(s) = h_s^p(s)u_s^p + h_s^q(s)u_s^q \quad (20)$$

and choose the shape functions as

$$h_r^p = \frac{L_i^{pq} - r}{L_i^{pq}}, \quad h_r^q = \frac{r}{L_i^{pq}}, \quad h_s^p = \frac{(L_i^{pq} - s)}{L_i^{pq}}, \quad h_s^q = \frac{s}{L_i^{pq}} \quad (0 \leq r, s \leq L_i^{pq}) \quad (21)$$

Then, the strain–displacement matrix \mathbf{B} becomes

$$\mathbf{B} = \frac{1}{L_i^{pq}} \begin{pmatrix} -1 & 0 & 1 & 0 \\ 0 & -1 & 0 & 1 \\ 0 & 0 & 0 & 0 \end{pmatrix} \quad (22)$$

If we choose the elasticity matrix \mathbf{D}_i^{pq} as

$$\mathbf{D}_i^{pq} = E_i^{pq} \begin{bmatrix} 1 & 0 & 0 \\ 0 & 1 & 0 \\ 0 & 0 & 0 \end{bmatrix} \quad (E: \text{Young's modulus}) \quad (23)$$

and assume the following limiting behaviour:

$$l_i^{pq} \equiv \lim_{L_i^{pq} \rightarrow 0} \frac{E_i^{pq} A_i^{pq}}{L_i^{pq}} \quad \text{and} \quad \lim_{L_i^{pq} \rightarrow 0} \alpha_i^{pq} = 0 \quad (24)$$

the stiffness matrix $k_{i,(p,q)}^{\text{link}}$ in Equation (19) becomes the identical to the stiffness matrix in Equation (17).

In this paper, the link stiffness l_i^{pq} is modelled as a function of γ_i^{pq} as

$$l_i^{pq} = l_0(\gamma_i^{pq})^n \quad (25)$$

where n is the penalty exponent used to push γ_i^{pq} to its bounds and l_0 is the upper bound of the link stiffness. The design variable γ_i^{pq} takes a positive value between γ_{Low} and γ_{Upper} :

$$0 < \gamma_{\text{Low}} \leq \gamma_i^{pq} \leq \gamma_{\text{Upper}} = 1 \quad (26)$$

For actual numerical implementation, γ_{Low} was set as 0.01 and the value of l_0 was 100–10⁴ times larger than the diagonal term of the stiffness matrix of the adjacent continuum element. The effects of involved parameters were studied in Reference [12]. A penalty exponent n between 2 and 3 was quite effective in obtaining clear optimal layouts; several numerical tests were performed to determine this exponent value. The continuation method applied to the magnitude of l_0 [12, 14] was also useful in obtained clear solid and void results.

Although six independent design variables in the connection i can be assigned to six individual links for stiffness control, it is convenient to use one unified design variable γ_i for every connection i and to define k_i^{link} for the assembled stiffness matrix at the connection i . When γ_i approaches γ_{Upper} , all nodes surrounding Connection i behave as if they are rigidly connected. On the other hands, when γ_i becomes γ_{Low} , all nodes behave as if they are disconnected. In this case, one can write the following:

$$k_{i,(p,q)}^{\text{link}}(\gamma_i) = l_i^{pq}(\gamma_i) k_{\text{nominal}}^{\text{link}} \quad (\text{for any } (p, q) \text{ combination}) \quad (27)$$

$$k_i^{\text{link}}(\gamma_i) \equiv \sum_{(p,q)} k_{i,(p,q)}^{\text{link}}(\gamma_i) \quad (28)$$

where $\sum_{(p,q)}$ implies the summation over all six link connections at Connection i .

If the ECP modelling technique is employed, the tangent stiffness matrix \mathbf{K}_{Tan} appearing in the incremental form of the equilibrium equation (11) should be replaced by

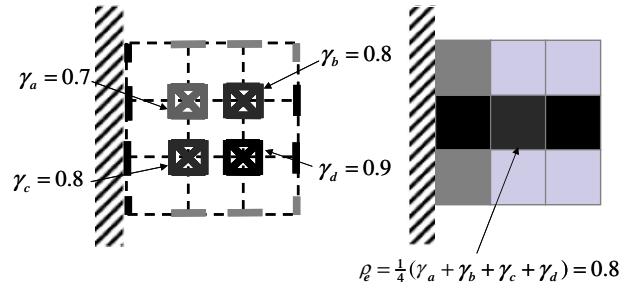
$$\mathbf{K}_{\text{Tan}} + \mathbf{K}^{\text{link}}(\gamma) \equiv \mathbf{K}_{\text{Tan}}^{\text{link}}(\gamma) \quad (29)$$

In (29), \mathbf{K}_{Tan} is the tangent stiffness matrix for nonlinear materials, but its assembly state is not the same as that of the tangent stiffness matrix in (11). This is because \mathbf{K}_{Tan} in (29) denotes the stiffness matrix for disconnected plane finite elements. The system link stiffness matrix $\mathbf{K}^{\text{link}}(\gamma)$ can be expressed as

$$\mathbf{K}^{\text{link}}(\gamma) = \sum_{i=1}^{\text{NC}} k_i^{\text{link}}(\gamma_i) \quad (30)$$

where NC is the total number of connections.

The disadvantage of the present ECP formulation is the increase in the total system matrix size due to links, which results in more computation time for calculating structure responses. However, the numerical difficulty such as stability can be enhanced as demonstrated in Reference [12] and the optimization formulation becomes much simpler. If an improved ECP formulation discussed in Reference [14] can be used for material-nonlinear problems, overall computation time can be substantially reduced.

Figure 5. Layout identification from a distribution of γ_i .

Before presenting the topology optimization formulation by ECP, we will briefly explain how to represent topological layouts corresponding to obtained distributions of γ_i . The easiest approach is the raster imaging scheme illustrated in Figure 5. In the raster imaging technique, the values of the design variable γ_i are used to render patches to obtain similar raster pictures in the conventional topology optimization. If an e th element is surrounded by four connections having the design variables, γ_a , γ_b , γ_c , and γ_d , their average will be considered as the element ρ_e for rendering:

$$\rho_e = \frac{1}{4}(\gamma_a + \gamma_b + \gamma_c + \gamma_d) \quad (31)$$

Equation (31) is also used to compute the element volume or mass when a mass constraint is imposed in an optimization problem.

2.4. Topology optimization formulation by ECP for the nonlinear continuum structure without unloading

Employing the ECP method for topology optimization, it is necessary to reformulate the optimization problem in terms of the new design variables γ as

$$\text{minimize} \quad \Phi(\gamma) = - \int_{\Omega} \int_{\hat{\varepsilon}} \boldsymbol{\sigma}^T d\boldsymbol{\varepsilon} d\Omega \quad (32a)$$

$$\text{subject to} \quad Q(\gamma) = \sum_{e=1}^{NE} \rho_e(\gamma) v_e - M_0 \leq 0 \quad (32b)$$

where $\hat{\varepsilon}$ is the induced strain by the displacement loading condition.

In this investigation, nonlinear problems without unloading will be considered. When loading is considered, the monotonically incremental displacement loading condition will be used [8, 10]. The overall optimization process is depicted in Figure 6. To facilitate the numerical calculation of the objective function, one may use a different form. By referring to the problem in Figure 7(a), for instance, $\Phi(\gamma)$ can be written as

$$\Phi = - \int_{\Omega} \int_{\hat{\varepsilon}} \boldsymbol{\sigma}^T d\boldsymbol{\varepsilon} d\Omega = - \int_0^{u_A} P_A du \approx - \sum_{m=1}^{N_{\text{inc}}} \Delta \Xi_m \quad (33)$$

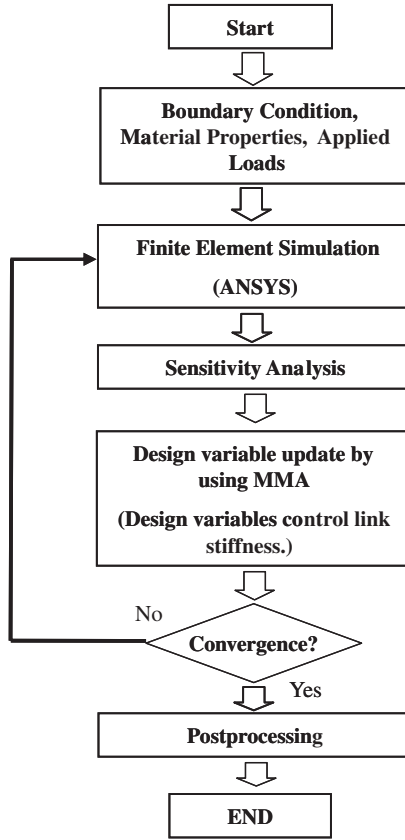


Figure 6. The developed optimization process using the element connectivity parameterization method.

with

$$\Delta \Xi_1 = \left(\frac{1}{2} P_A^1 \right) \Delta u_A, \quad \Delta \Xi_m = \frac{1}{2} (P_A^m + P_A^{m-1}) \Delta u_A, \quad \Delta u_A = \frac{u_A}{N_{\text{inc}}}$$

where N_{inc} is the number of the incremental loads in the Newton–Raphson iteration. The symbols u_A and P_A^m denote the prescribed displacement and the reaction force at the m th incremental displacement load at the loading point A. In this paper, $N_{\text{inc}} = 10$ –30 was tested and used for all numerical examples considered.

To calculate the sensitivity of the objective function Φ in (32a) with respect to the design variable γ_i , the procedure used to derive Equation (13) can be equally applied for the ECP implementation. Specifically,

$$\frac{\partial \Phi}{\partial \gamma_i} = - \lim_{\Omega_i \rightarrow 0} \frac{\partial}{\partial \gamma_i} \int_{\Omega_i} \int_{\hat{\mathbf{e}}} \boldsymbol{\sigma}^T d\boldsymbol{\varepsilon} d\Omega = - \lim_{\Omega_i \rightarrow 0} \int_{\Omega_i} \int_{\hat{\mathbf{e}}} \int_{\boldsymbol{\varepsilon}} d\boldsymbol{\varepsilon}^T \frac{\partial(\mathbf{D}_i)}{\partial \gamma_i} d\boldsymbol{\varepsilon} + 2 \left(\frac{\partial(d\boldsymbol{\varepsilon})}{\partial \gamma_i} \right)^T \mathbf{D}_i d\boldsymbol{\varepsilon} d\Omega \quad (34)$$

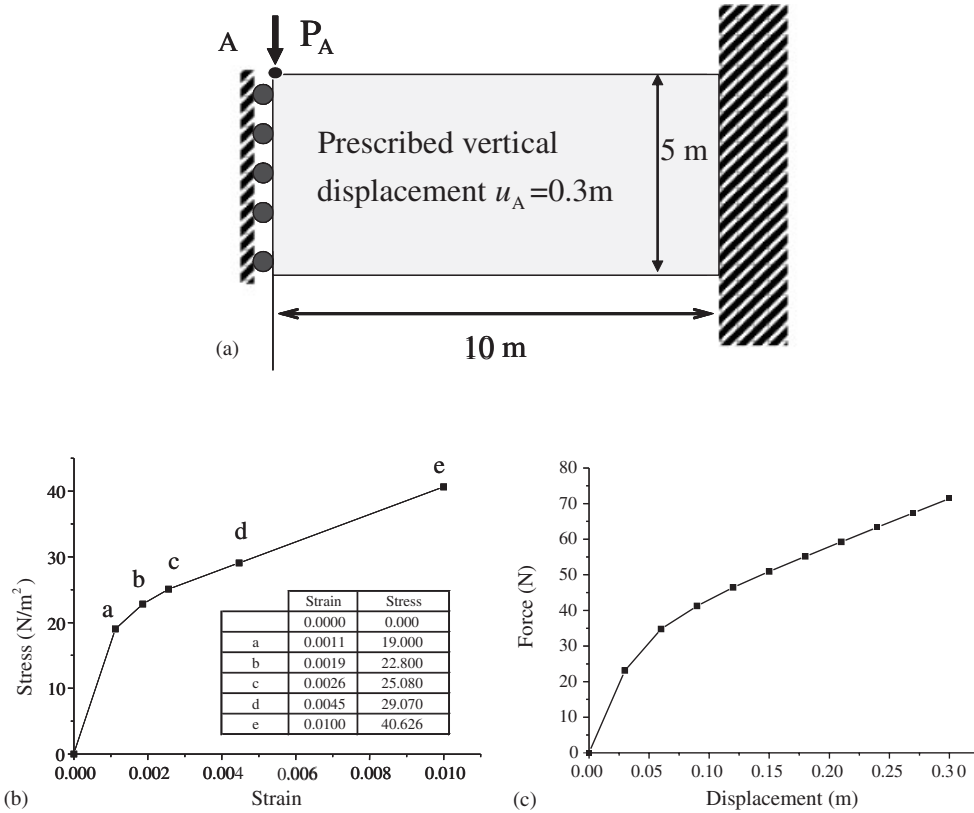


Figure 7. A test problem for verifying the derived analytic sensitivity: (a) problem definition; (b) the elastoplastic material model; and (c) load-displacement curve.

where Ω_i and \mathbf{D}_i denote the region occupied by all links and the elasticity matrix of the links in Equation (23) at Connection i . Equation (34) can be rewritten as

$$\frac{\partial \Phi}{\partial \gamma_i} = \lim_{\Omega_i \rightarrow 0} \int_{\Omega_i} \int_{\hat{\mathbf{\epsilon}}} \int_{\mathbf{\epsilon}} d\mathbf{\epsilon}^T \frac{\partial(\mathbf{D}_i)}{\partial \gamma_i} d\mathbf{\epsilon} d\Omega - 2 \int_{\Gamma} \int_{\hat{\lambda}_{LF}} \int_{\hat{\mathbf{u}}} \frac{\partial(d\lambda_{LF})}{\partial \gamma_i} \hat{\mathbf{t}}^T d\mathbf{u} d\Gamma \quad (35)$$

Now from

$$d\boldsymbol{\sigma} = \mathbf{D}_i(\gamma_i) d\boldsymbol{\epsilon} \quad (36)$$

one can write

$$\frac{\partial(d\boldsymbol{\sigma})}{\partial \gamma_i} = \frac{\partial(\mathbf{D}_i)}{\partial \gamma_i} d\boldsymbol{\epsilon} + \mathbf{D}_i \frac{\partial(d\boldsymbol{\epsilon})}{\partial \gamma_i} \quad (37)$$

With the assumptions of the monotonic displacement loading condition and the design-independent traction condition, the following condition can be obtained:

$$\int_{\Gamma} \hat{\mathbf{t}}^T d\mathbf{u} d\Gamma = \int_{\Gamma} d\mathbf{u}^T \hat{\mathbf{t}} d\Gamma = \text{constant} \rightarrow \int_{\Gamma} (\partial d\mathbf{u} / \partial \gamma_i)^T \hat{\mathbf{t}} d\Gamma = 0 \quad (38)$$

Table I. The comparison of the analytic sensitivity and the derived sensitivity of Equation (42) (for the finite difference, design perturbation = 10^{-4}).

Design variable no	Analytical sensitivity by Equation (42)	Sensitivity by finite difference	Difference (%)
5	0.2706	0.2754	−1.77
12	0.3789	0.3749	1.06
30	0.1665	0.1678	−0.78
35	0.0881	0.0890	−1.02

Unloading is not considered.

If the test function fields in the incremental form of Equation (7) are chosen as $\delta \mathbf{u} \rightarrow \partial \mathbf{u} / \partial \gamma_i$ and $\delta \boldsymbol{\varepsilon} \rightarrow \partial \boldsymbol{\varepsilon} / \partial \gamma_i$ and condition (38) is used, the following equation can be obtained:

$$0 = d\lambda_{LF} \int_{\Gamma} (\partial(\mathbf{d}\mathbf{u}) / \partial \gamma_i)^T \hat{\mathbf{t}} d\Gamma - \lim_{\Omega_i \rightarrow 0} \int_{\Omega_i} \partial \mathbf{d}\boldsymbol{\varepsilon} / \partial \gamma_i^T d\boldsymbol{\sigma} d\Omega \quad (39)$$

$$\lim_{\Omega_i \rightarrow 0} \int_{\Omega_i} \partial \mathbf{d}\boldsymbol{\varepsilon} / \partial \gamma_i^T d\boldsymbol{\sigma} d\Omega = 0 \quad (40)$$

Using Equation (40), the differential of the load factor λ_{LF} with respect to the design variable can be given as

$$\frac{\partial d\lambda_{LF}}{\partial \gamma_i} = \lim_{\Omega_i \rightarrow 0} \int_{\Omega_i} d\boldsymbol{\varepsilon}^T \frac{\partial \mathbf{D}_i}{\partial \gamma_i} d\boldsymbol{\varepsilon} d\Omega / d\mathbf{u}^T \hat{\mathbf{t}} \quad (41)$$

Combining (41) and (35) yields the sensitivity of Φ with respect to γ_i :

$$\begin{aligned} \frac{\partial \Phi}{\partial \gamma_i} &= - \lim_{\Omega_i \rightarrow 0} \int_{\Omega_i} \int_{\hat{\varepsilon}} \int_{\varepsilon} d\boldsymbol{\varepsilon}^T \frac{\partial \mathbf{D}_i}{\partial \gamma_i} d\boldsymbol{\varepsilon} d\Omega \\ &= -u_i^T \frac{dk_i^{\text{link}}}{d\gamma_i} u_i \end{aligned} \quad (42)$$

where u_i denotes the converged displacement vector of the links at Connection i . The final sensitivity expression in (42) is simple and does not involve any material-dependent term explicitly. Therefore, there is no need to penalize several material-dependent parameters unlike in the density-based method.

As depicted in Figure 6, the method of moving asymptotes and the optimality criterion are used as optimizers [30]. To verify the validity of the derived sensitivity expression, comparison is made between the result by (42) and the sensitivity by the direct finite-differencing scheme for the test problem shown in Figure 7. The design domain is discretized by 25 plane stress elements. By ECP, the total number of design variables is 112. The numerical values of $\partial \Phi / \partial \gamma_i$ for $u_A = 0.3$ m are listed in Table I, which confirms the validity of the present sensitivity expression.

3. ECP TOPOLOGY OPTIMIZATION OF NONLINEAR PROBLEMS

In this section, the ECP formulation developed in the previous section will be applied to the topology design optimization of: (1) multilinear elastoplastic small-displacement continua, (2) hyperelastic

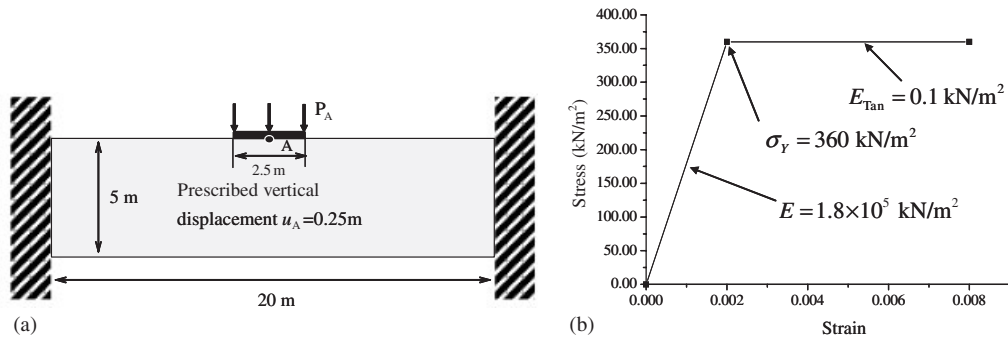


Figure 8. Topology optimization involving a bilinear elastoplastic material: (a) problem description (mesh: 80×20 , mass constraint ratio = 25%); and (b) bilinear elastoplastic material model ($\nu = 0.0$ used).

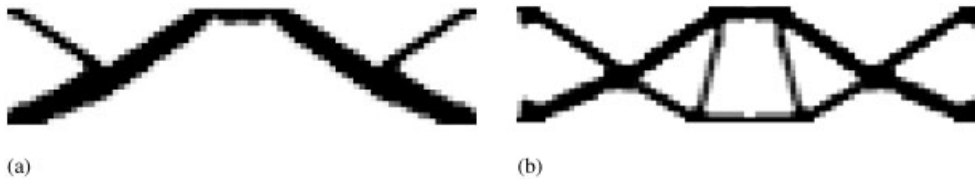


Figure 9. The optimized layouts obtained by the ECP formulation for the problem depicted in Figure 8(a): (a) the result for the linear elastic material model; and (b) the result for the bilinear elastoplastic material model in Figure 8(b).

(Mooney–Rivlin) large displacement continua. Since the effectiveness of the ECP method in the topology optimization for linear elastic, small or large displacement continua has already been verified in Reference [12], the validity of the proposed ECP formulation for material-nonlinearity will be mainly investigated here. To suppress checkerboard patterns, the filtering technique explained in Reference [12], an extension of the filtering method developed for the density method [2] is used for all numerical problems considered in this work. Since the gradient-based optimization formulation used does not guarantee the global optimal solution, a parameter set yielding satisfactory results is selected after several tests.

3.1. Case 1: Bilinear elastoplastic material-nonlinearity

As the first case study, we considered the same problem solved in References [8, 10]. The design domain, boundary and loading conditions are depicted in Figure 8(a). The bilinear elastoplastic stress–strain relation is also given in Figure 8(b). The objective function is given by Φ in Equation (32a).

The optimized result obtained by the ECP formulation for the bilinear elastoplastic model with the penalty exponent $n=3$ is shown in Figure 9(b). The topological layout in Figure 9(b) is almost identical to that obtained in References [8, 10]. It will be interesting to compare the optimal layout (Figure 9(b)) based on the elastoplastic model and the layout (Figure 9(a)) based on the linear elastic model ($E = 1.8 \times 10^5$ kN/m², $\nu = 0.0$). To compare the structural efficiency

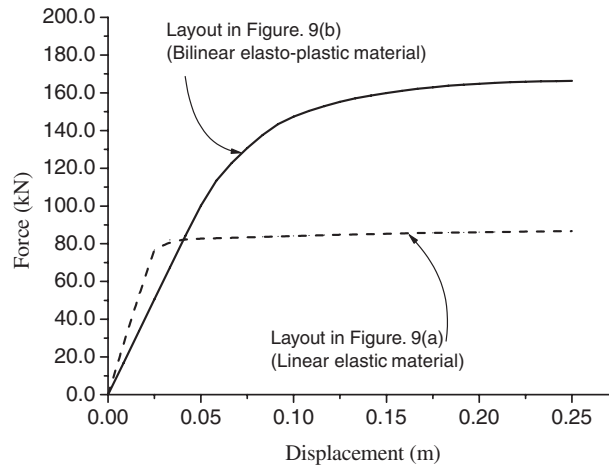


Figure 10. The nonlinear load–displacement curves for the optimized layouts with the linear elastic and the bilinear elastoplastic material models.

of the design in Figure 9(a) and that of the design in Figure 9(b), the analyses based on the bilinear elastoplastic model were carried out for the two designs and the results are plotted in Figure 10. As expected, the stiffness dP_A/du_A of the optimized layout based on the bilinear elastoplastic model is smaller in the elastic range, but larger in the plastic range than that of the optimized layout based on the pure elastic model. The intermediate layouts and the final optimized layout are plotted in Figure 11 that shows the convergence behaviour of the proposed method.

3.2. Case 2: Multilinear elastoplastic material-nonlinearity

As the second case study, the topology design optimization of a continuum structure having multilinear elastoplastic material-behaviour was considered. To focus on the material nonlinearity, kinematic nonlinearity was not considered here.

The examination of the material behaviour depicted in Figure 12(b) indicates that the standard element density method would require several interpolation functions to penalize all the material characterizing parameters. However, no such difficulty appears in the present ECP formulation.

Figure 13(a) compares the optimized layouts obtained by using the linear elastic material model and the multilinear elastoplastic model with the penalty exponent $n = 3$. As in Case 1, a structure having more members, including the two vertical members in the middle, is obtained when the nonlinear elastoplastic material behaviour is considered. The nonlinear load–displacement curves shown in Figure 13(b) confirm that for large displacement, the structural efficiency of the optimized layout obtained for the multilinear elastoplastic material is superior to that of the linear result. To study the effect of the different input displacements on the optimized layouts, the input displacement was varied from 0.1 to 4 m and the results are plotted in Figure 14. Figure 14 clearly shows the effect of the displacement input magnitude on the topology connectivity of the optimized layout.

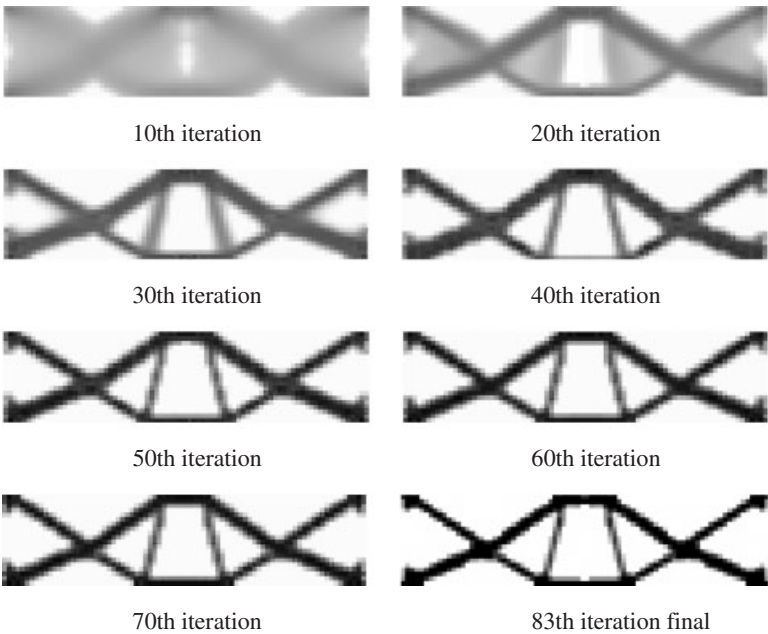


Figure 11. Layout appearing during the optimization process for the problem depicted in Figure 8.

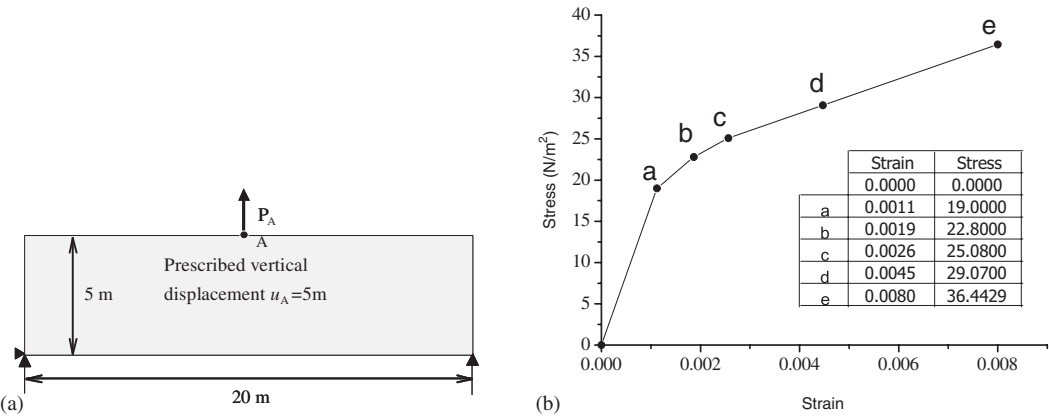


Figure 12. Topology optimization for a multilinear elastoplastic material: (a) problem description (mesh: 80×20 , mass constraint ratio = 25%); and (b) multilinear elastoplastic material model ($\nu = 0.3$ used).

3.3. Case 3: Hyperelastic material-nonlinearity

As the last case study, the topology design optimization problems involving nonlinear hyper elastic materials illustrated in Figure 15 were considered. With this case study, the usefulness of the proposed ECP formulation can be demonstrated in optimization problems involving

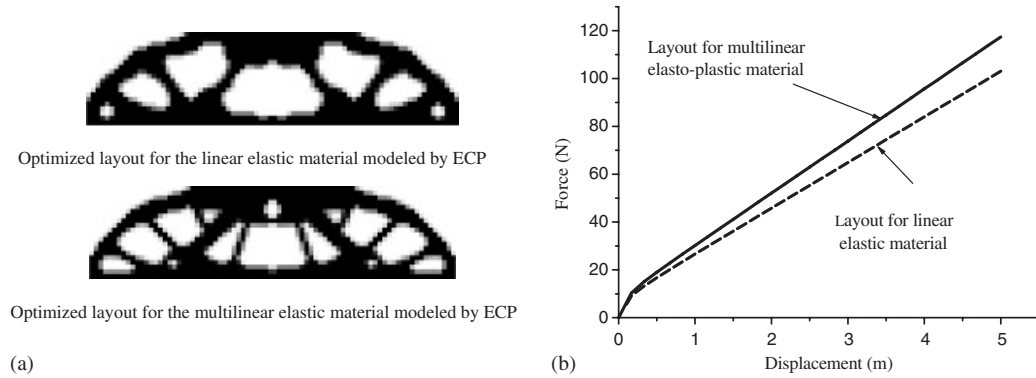


Figure 13. The comparison of the optimized results for the problem depicted in Figure 12(a) for the linear elastic and multilinear elastoplastic models: (a) comparison of the optimal layouts; and (b) the nonlinear load–displacement curves for the layouts shown in (a).

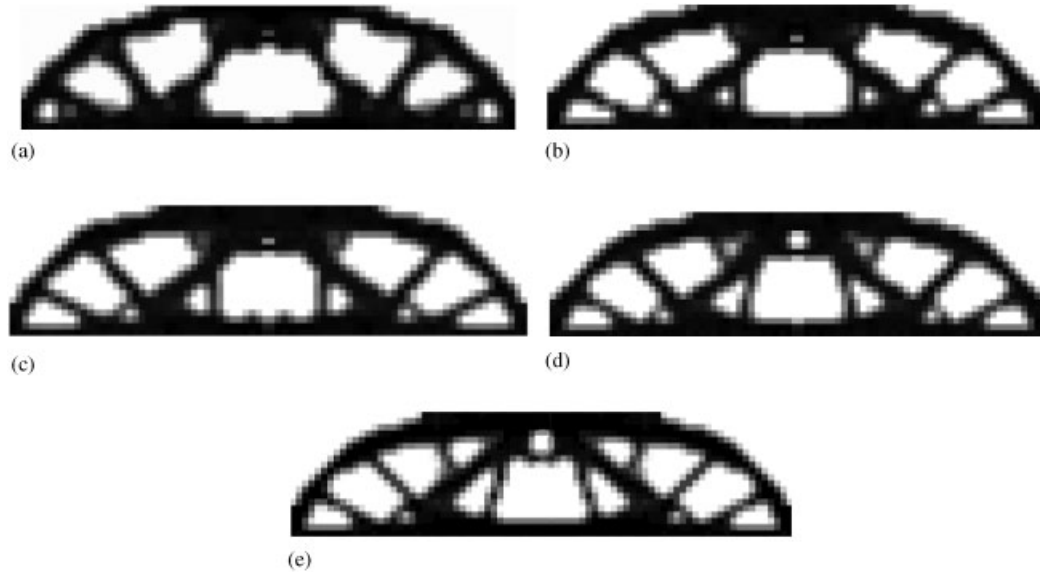


Figure 14. The optimized results for various input displacements (u_A): (The material model used is the multilinear elastoplastic model in Figure 12(b).) (a) $u_A = 0.1$; (b) $u_A = 1$; (c) $u_A = 2$; (d) $u_A = 3$; and (e) $u_A = 4$.

material and kinematic nonlinearities. For this case, the following Mooney–Rivlin material model was employed:

$$W = c_1(\bar{I}_1 - 3) + c_2(\bar{I}_2 - 3) \quad (W : \text{Strain energy density}) \quad (43)$$

$$\bar{I}_1 = I_3^{-1/3} I_1, \quad \bar{I}_2 = I_3^{-2/3} I_2, \quad \bar{I}_3 = I_3^{-1/2} I_3 \quad (44)$$

$$I_1 = C_{ij}, \quad I_2 = \frac{1}{2}(I_1^2 - C_{ij}C_{ij}), \quad I_3 = \det(C_{ij}) \quad (45)$$

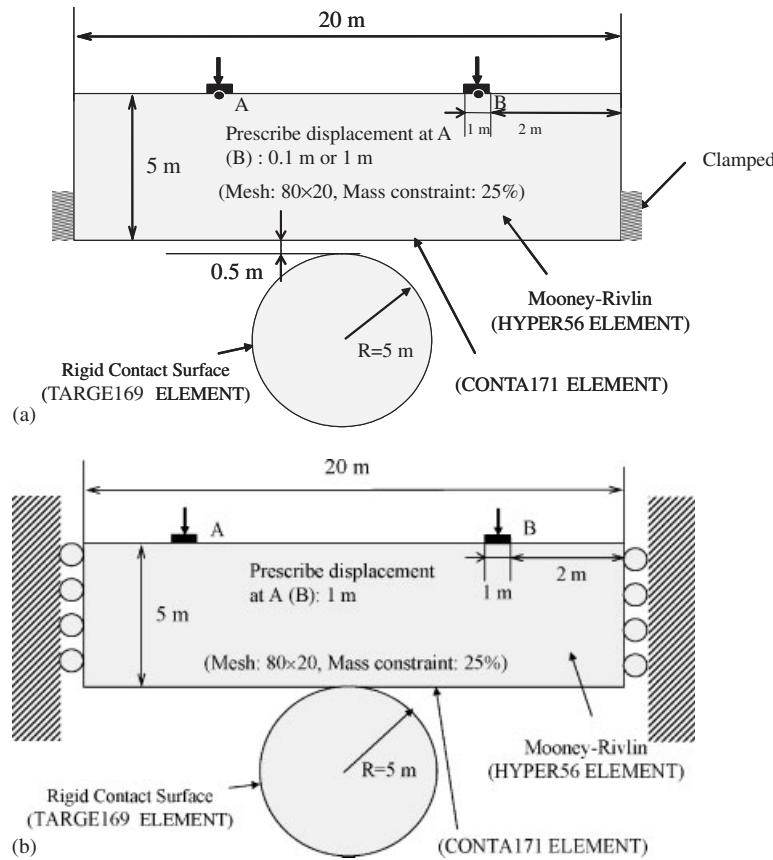


Figure 15. The topology optimization of hyperelastic continuum structures. The Mooney–Rivlin model (with $c_1 = 0.293 \text{ J}$, $c_2 = 0.177 \text{ J}$ in Equation (43)) is employed. The bottom surface of the design domain may contact with a rigid circular body.

where c_1 and c_2 are the material characteristic constants for the Mooney–Rivlin material. The relation between the Cauchy–Green strain tensor C_{ij} and the second Piola–Kirchoff stress S_{ij} is given by

$$S_{ij} = 2 \frac{\partial W}{\partial C_{ij}} \quad (46)$$

In case of the hyperelastic material modelled by (43), not only the material-nonlinearity but also the kinematic nonlinearity should be considered [26, 27]. If the SIMP method were employed, the two parameters c_1 and c_2 in (43) might be interpolated as the penalized functions of the element density variable. Even with an appropriate combination of the penalty exponents of the interpolation functions, the numerical instability resulting from low-density elements for kinematic nonlinear analysis would occur if the element density method were used. However, no such difficulty appears when the ECP is employed [12].

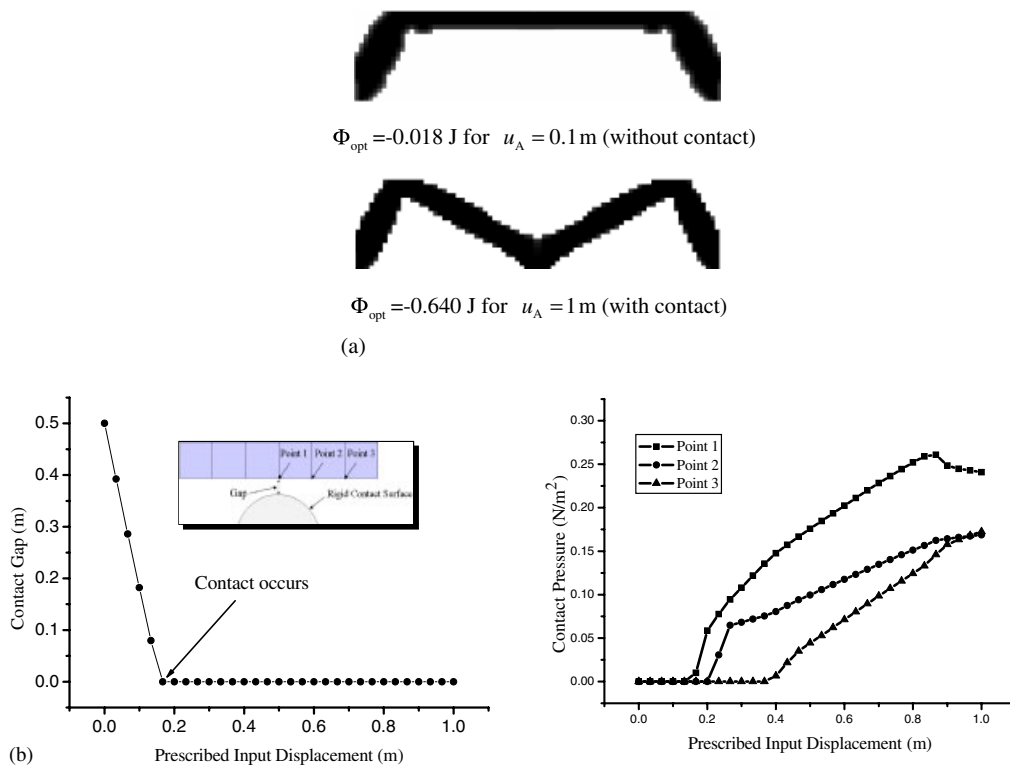


Figure 16. The optimized results for topology optimization problem depicted in Figure 15(a): (a) the optimal layouts for $u_A = 0.1$ and 1 m; and (b) the detailed contact phenomena at a few points of the bottom surface of the loaded optimal layout for $u_A = 1$ m.

As may be understood from the problem definition in Figure 15, the bottom surface of the design domain can contact with a rigid circular body. The objective function for the problems is the ductility as in previous cases. All analyses including the sensitivity analysis were performed by ANSYS and the used elements are CONTACT171, TARGET 169, and HYPER56. When contact analysis was necessary, the normal contact stiffness factor was set as 3.0 and other controlling parameters were default values provided by ANSYS. (The friction between two bodies was ignored.) The displacement loading conditions were used (see Reference [24] for numerical contact analysis).

(A) Numerical results for the problem depicted in Figure 15(a). Two displacement loading cases, $u_A (= u_B) = 0.1$ m and $u_A (= u_B) = 1$ m, were considered. In case of $u_A = 0.1$ m, no contact between two bodies will occur. In case of $u_A = 1$ m, however, the contact must be considered. The optimized layouts for $u_A = 0.1$ and 1 m obtained by the present ECP formulation are shown in Figure 16(a). For this problem, the penalty exponent of $n = 2$ was used. The obtained layouts agree well with our physical intuition.

In Figure 16(b), the gap distance between the rigid circular body and Point 1 of the optimized layout obtained for $u_A = 1$ m is plotted. When the prescribed displacement u_A reached 0.1666 m, the contact between the original layout and the rigid body occurred. The contact pressures developed at Points 1, 2 and 3 on the bottom surface of the optimal layout are also shown in Figure 16(b).

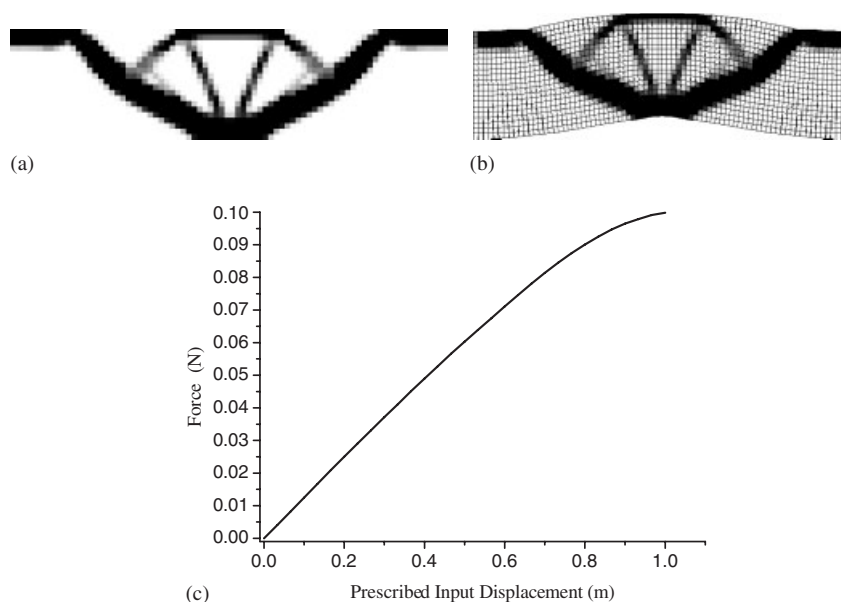


Figure 17. The optimized result for the topology optimization problem defined in Figure 15(b): (a) optimal layout; (b) deformed shape; and (c) the force–displacement curve.

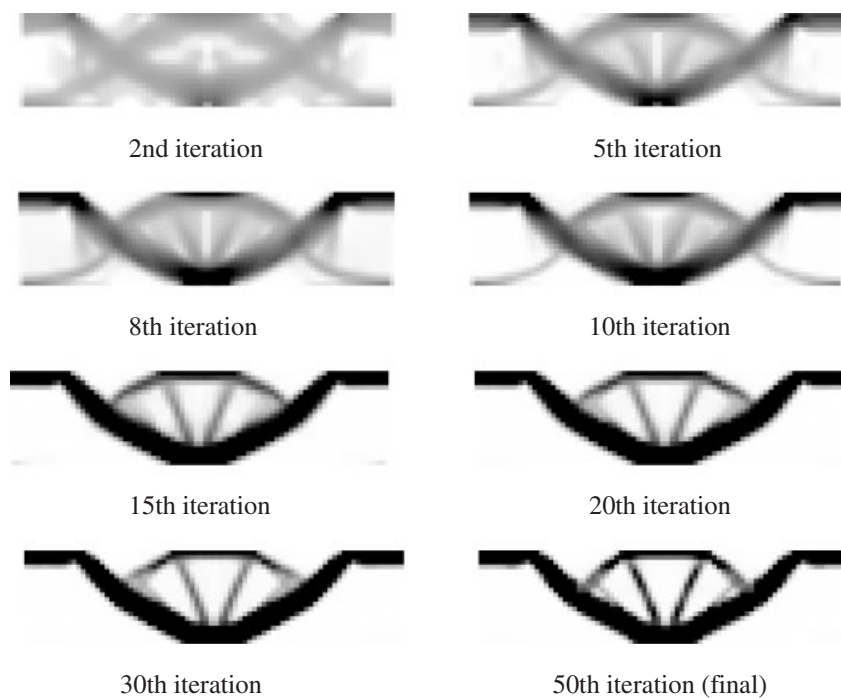


Figure 18. Layouts appearing during the optimization process for the problem depicted in Figure 15(b).

This graph shows that the contact started at Point 1 and proceeded to Point 3 via Point 2, which physically makes sense.

(B) Numerical results for the problem depicted in Figure 15(b). In this case, the bottom surface of the hyperelastic body is always in contact with the rigid body. The prescribed displacement at A is 1 m. The optimized result is shown in Figure 17(a) and the deformed shape, in Figure 17(b). The nonlinear load–displacement curve is also plotted in Figure 17(c). Some intermediate layouts and the final layout are plotted in Figure 18.

4. CONCLUSIONS

The topology optimization involving material-nonlinearity without unloading was formulated by the ECP method. Multilinear elastoplastic problems and the Mooney–Rivlin hyperelastic problems were solved to demonstrate the effectiveness of the ECP method. Because the stiffness of linear elastic links connecting material-nonlinear continuum elements is interpolated in the ECP formulation, sensitivity analysis is considerably simpler than that for the standard density approach. In fact, commercial software capable of dealing with the involved nonlinearity was used for analytic sensitivity calculation. Although simple boundary contact was considered, the ECP method handled the hyper-elastic problem involving boundary contact. If the developed ECP method is extended for problems involving unloading, various design problems such as crashworthiness may be effectively solved.

REFERENCES

1. Bendsøe MP, Kikuchi N. Generating optimal topologies in structural design using a homogenization method. *Computer Methods in Applied Mechanics and Engineering* 1988; **71**:197–224.
2. Bendsøe MP, Sigmund O. *Topology Optimization Theory, Methods and Applications*. Springer: New York, 2003.
3. Yuge K, Kikuchi N. Optimization of a frame structure subjected to a plastic deformation. *Structural Optimization* 1995; **10**:197–208.
4. Pedersen CBW. Crashworthiness design of transient frame structures using topology optimization. *Computer Methods in Applied Mechanics and Engineering* 2004; **193**(6–8):653–678.
5. Pedersen CBW. Topology optimization of 2D-frame structures with path dependent response. *International Journal for Numerical Methods in Engineering* 2003; **57**(10):1471–1501.
6. Kaliszky S, Lógó J. Optimal strengthening of elastoplastic trusses with plastic deformation and stability constraints. *Structural and Multidisciplinary Optimization* 1999; **18**(4):296–299.
7. Soto CA. Structural topology optimization for crashworthiness. *International Journal for Crashworthiness* 2004; **9**(3):277–283.
8. Schwarz S, Maute K, Ramm E. Topology and shape optimization for elastoplastic structural response. *Computer Methods in Applied Mechanics and Engineering* 2001; **190**:2135–2155.
9. Pedersen CBW. Revisiting topology optimization of continuum structures with elastoplastic response. *Published in 15th Nordic Seminar on Computational Mechanics*, Aalborg, Denmark, 2002.
10. Maute K, Schwarz S, Ramm E. Adaptive topology optimization of elastoplastic structures. *Structural Optimization* 1998; **15**:81–91.
11. Swan CC, Kosaka I. Voigt–Reuss topology optimization for structures with nonlinear material behaviours. *International Journal for Numerical Methods in Engineering* 1997; **40**:3785–3814.
12. Yoon GH, Kim YY. Element connectivity parameterization for topology optimization of geometrically nonlinear structures. *International Journal of Solids and Structures* 2005; **42**(7):1983–2009.
13. Yoon GH, Kim YY. The element connectivity parameterization formulation for the topology design optimization of multiphysics systems. *International Journal for Numerical Methods in Engineering* 2005; **64**:1649–1677.

14. Yoon GH, Joung YS, Kim YY. Optimal layout design of three-dimensional geometrically nonlinear structures using the element connectivity parameterization method. *International Journal for Numerical Methods in Engineering* 2005, in press.
15. Tsay JJ, Arora JS. Nonlinear structural design sensitivity analysis for path dependent problems. Part 1: general theory. *Computer Methods in Applied Mechanics and Engineering* 1990; **81**:183–208.
16. Michaleris P, Tortorelli DA, Vidal CA. Tangent operators and design sensitivity formulations for transient nonlinear coupled problems with applications to elastoplasticity. *International Journal for Numerical Methods in Engineering* 1994; **37**(14):2471–2499.
17. Hilding D, Klarbring A, Petersson J. Optimization of structures in unilateral contact. *Applied Mechanics Reviews* 1999; **52**:139–160.
18. Lee TH, Arora JS. A computational method for design sensitivity analysis of elastoplastic structures. *Computer Methods in Applied Mechanics and Engineering* 1995; **122**:27–50.
19. Joung YS, Yoon GH, Kim YY. Lumped mass modeling for local-mode-suppressed element connectivity parameterized topology optimization of vibrating structures. *6th World Congress on Structural and Multidisciplinary Optimization*, Rio de Janeiro, Brazil, 2005.
20. *ANSYS User's Manual*. Swanson Analysis Systems, Inc., Houston, PA, 1995.
21. Petersson J, Patriksson M. Topology optimization of sheets in contact by a subgradient method. *International Journal for Numerical Methods in Engineering* 1997; **40**(7):1295–1321.
22. Petersson J. On stiffness maximization of variable thickness sheet with unilateral contact. *Quarterly of Applied Mathematics* 1996; **54**(3):541–550.
23. Mankame ND, Ananthasuresh GK. Topology optimization for synthesis of contact-aided compliant mechanisms using regularized contact modeling. *Computers and Structures* 2004; **82**(15–16):1267–1290.
24. Wriggers P. *Computational Contact Mechanics*. Wiley: New York, 2002.
25. Folgado J, Fernandes PR, Rodrigues H. Topology optimization of three-dimensional structures under contact conditions. *Published in WCSMO-4; Forth World Congress on Structural and Multidisciplinary Optimization*, Dalian, China, 2001.
26. Bathe KJ. *Finite Element Procedures*. Prentice-Hall: Englewood Cliffs, NJ, 1996.
27. Owen DRJ, Hinton E. *Finite Elements in Plasticity: Theory and Practice*. Pineridge Press: Swansea, U.K., 1980.
28. Bruns TE, Tortorelli DA. An element removal and reintroduction strategy for the topology optimization of structures and compliant mechanisms. *International Journal for Numerical Methods in Engineering* 2003; **57**(10):1413–1430.
29. Cho SH, Jung HS. Design sensitivity analysis and topology optimization of displacement-loaded nonlinear structures. *Computer Methods in Applied Mechanics and Engineering* 2003; **192**:2539–2553.
30. Svanberg K. The method of moving asymptotes—a new method for structural optimization. *International Journal for Numerical Methods in Engineering* 1987; **24**:359–373.